nature materials

ARTICLES

PUBLISHED ONLINE: 9 SEPTEMBER 2012 | DOI: 10.1038/NMAT3406

Ultrasensitive detection of toxic cations through changes in the tunnelling current across films of striped nanoparticles

Eun Seon Cho[1,2†], Jiwon Kim[3†], Baudilio Tejerina[3], Thomas M. Hermans[3], Hao Jiang[4], Hideyuki Nakanishi[3], Miao Yu[2], Alexander Z. Patashinski[3], Sharon C. Glotzer[4], Francesco Stellacci[1,2*] and Bartosz A. Grzybowski[3*]

Although multiple methods have been developed to detect metal cations, only a few offer sensitivities below 1 pM, and many require complicated procedures and sophisticated equipment. Here, we describe a class of simple solid-state sensors for the ultrasensitive detection of heavy-metal cations (notably, an unprecedented attomolar limit for the detection of CH_3Hg^+ in both standardized solutions and environmental samples) through changes in the tunnelling current across films of nanoparticles (NPs) protected with striped monolayers of organic ligands. The sensors are also highly selective because of the ligand–shell organization of the NPs. On binding of metal cations, the electronic structure of the molecular bridges between proximal NPs changes, the tunnelling current increases and highly conductive paths ultimately percolate the entire film. The nanoscale heterogeneity of the structure of the film broadens the range of the cation-binding constants, which leads to wide sensitivity ranges (remarkably, over 18 orders of magnitude in CH_3Hg^+ concentration).

Many cations are toxic, posing serious consequences for the environment and for human health. As an example, organomercury species (for instance, methylmercury (II); refs 1,2) are extremely dangerous and cause neurological disorders such as Minamata disease[3,4], and cadmium poisoning results in kidney and/or liver failure, bone softening and other ill effects (for example, Itai-itai disease[5,6]). Therefore, sensitive and selective detection of toxic metal cations is of paramount importance in assessing water pollution and in the elimination of potentially serious health and environmental hazards[7–9]. There are multiple approaches to detect these ions, including atomic absorption spectroscopy[10,11] and inductively coupled plasma spectroscopy[12,13] (ICP), a host of optical methods (colorimetric[14,15] or fluorescence-based assays[16,17] and systems based on surface plasmon resonance[18,19] or surface-enhanced Raman scattering[20,21]), and electrochemical methods[22,23]. Frequently, however, these methods require a sophisticated chemistry to incorporate host materials, such as macrocyclic rings (crown ethers, calixarenes or porphyrins), metal-ion-recognizable proteins, nucleic acids and polymers. Moreover, the sensitivity of these methods is insufficient[24–27] in several situations of public health concern (for example, accumulation of low picomolar concentrations of CH_3Hg^+ and Cd^{2+} in fish[28,29]). Furthermore, host–guest chemistries are not available for all cations, with CH_3Hg^+ being a prominent example[2].

Here we show that gold nanoparticles (Au NPs) coated with binary mixtures of *n*-hexanethiol (HT) and alkanethiols terminated with $n = 1$, 2 or 3 ethylene glycol (EG) units have a striped ligand structure (Fig. 1a,b) that generates supramolecular pockets able to selectively trap ions, and that on such trapping the electron-conduction mechanism through films of these NPs changes markedly[30]. We implement these findings in a solid-state sensor of unmatched sensitivity: HT/EG_3 NPs sense CH_3Hg^+ selectively and with a detection limit of ~1 aM, HT/EG_2 NPs sense ~1 pM concentrations of Cd^{2+}, and HT/EG_1 NPs are ~1 nM sensors for Zn^{2+}.

Au NPs ($d = 4.7 \pm 0.9$ nm) were synthesized as described previously[31,32] (see Methods) and were functionalized with alternating stripes (Fig. 1a) of HT and EG_n thiols (HS–$(CH_2)_6$–$(OCH_2CH_2)_n$–OH, ultrapure grade, ProChimia). These striped NPs were examined by scanning tunnelling microscopy (STM): the width of both HT and EG_2 stripes was ~1.3 ± 0.1 nm (Fig. 1b). For control experiments, we prepared NPs coated with disordered HT/EG_n mixed self-assembled monolayers (SAMs; random NPs (ref. 33)), but with the same relative content of the two thiols as in the striped NPs (see Supplementary Section S1), and also NPs covered with one-component SAMs of EG_n thiols. All types of NPs were dispersed in methanol with a concentration of 2 mM of Au atoms. To fabricate the sensors, Au electrodes (30 nm thick, 5 mm long) were sputter-coated onto a glass substrate using a shadow mask; the gap between the two electrodes was typically $w = 50$ μm wide and $l = 5$ mm long (Fig. 1c). Approximately 3 μl of the Au NP solution was drop-cast onto the patterned glass and dried for two days in vacuum conditions to give NP films about $H \sim 150$ nm thick (determined by profilometry for each sample); in this way, the number of NPs between the electrodes was of the order of 10^{11} (Fig. 1d). To prevent re-dissolution of the film on exposure

[1]Department of Materials Science and Engineering, Massachusetts Institute of Technology, Cambridge, Massachusetts 02139, USA, [2]Institute of Materials, Ecole Polytechnique Fédérale de Lausanne (EPFL), 1015, Switzerland, [3]Department of Chemical and Biological Engineering and Department of Chemistry, Northwestern University, 2145 Sheridan Road, Evanston, Illinois 60208, USA, [4]Department of Chemical Engineering and Department of Materials Science and Engineering, University of Michigan, Ann Arbor, Michigan 48109-2136, USA. †These authors contributed equally to this work. *e-mail: francesco.stellacci@epfl.ch; grzybor@northwestern.edu.

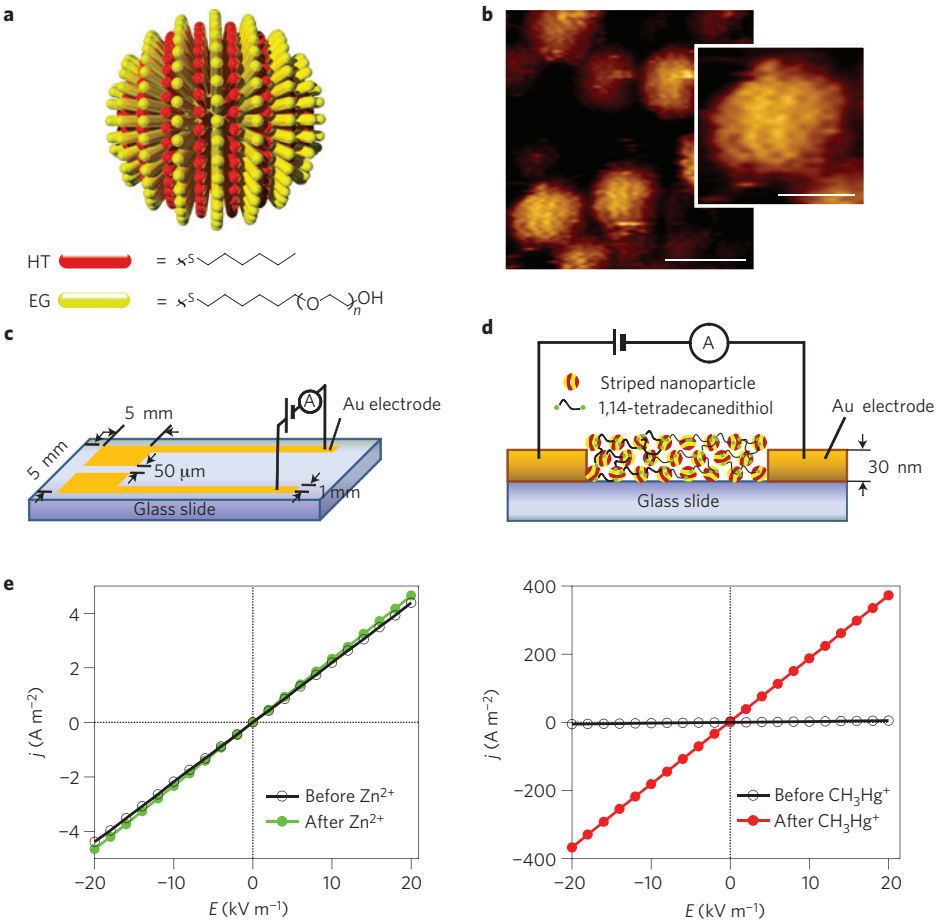

Figure 1 | Experimental set-up and typical *j–E* plots. a,**b**, An idealized scheme of a striped nanoparticle (**a**) and the corresponding STM image (here, for HT/EG_2 NPs) obtained by a Veeco multimode scanning probe microscope on a vibration damping table (in an acoustic chamber, at room temperature, and in air; **b**). Scale bars, 10 nm (main image) and 5 nm (inset). **c**,**d**, The scheme and the dimensions of the device (**c**) and the side view of the NP film (**d**). **e**, Ohmic current density versus applied field, *j–E*, and dependencies for a film of striped HT/EG_3 Au NPs before exposure to cations (black circles) and after exposure to cations (coloured circles). In the graph on the left, the conductance of the films is virtually unchanged after immersion in a 1 mM solution of Zn^{2+} (green circles). In the graph on the right, immersion of the same film in a 1 mM solution of CH_3Hg^+ (red circles) results in a marked change in the conductance (note the difference in the *j* ranges in the two plots).

to solvent, the film was reinforced by crosslinking the NPs with 1,14-tetradecanedithiol (dithiol concentration: 5 mM in toluene, crosslinking time: 40 min; for details see refs 34–36). Subsequently, the films were washed with an excess of toluene, dried under a stream of Ar, and then placed in vacuum conditions for two days. After drying the solvent, the Au electrodes were connected to a high-precision Keithley 6517 electrometer housed in a home-made Faraday cage (to minimize the effects of static electricity). The films were subsequently immersed in 2 ml of solutions of K^+, Na^+, Zn^{2+}, Cd^{2+}, Cs^+, CH_3Hg^+, Co^{2+}, Hg^{2+}, Pb^{2+}, Cu^{2+}, Ni^{2+}, Tl^+, Ca^{2+}, Ag^+ and CH_3Zn^+ chloride salts in ultrapure water (resistivity: 18.2 MΩ cm) with concentrations ranging from 1 mM down to 1 zM (zeptomolar, 10^{-21} M; note, the nature of the anions of the salts used, for example, chlorides versus bromides, had no effect on the results described below). The films were kept immersed in these solutions for $t \sim 120$ s. This time was sufficient for the ions to penetrate the full depth of the film, H—using a conservative estimate of the diffusion coefficient of ions/small molecules in a nanoporous material, $D \sim 10^{-14}$ m^2 s^{-1} (ref. 37), the diffusion depth can be estimated as $\sqrt{Dt} \sim 1\,\mu$m, which is greater than H. Consequently, the conductivities of the films discussed below did not change for longer immersion times. After immersion, the films were washed with copious amounts of water to remove excess salt and were then thoroughly dried under a stream of nitrogen. All subsequent measurements were performed at room temperature ($T \sim 300 \pm 2$ K), under dry air in a hermetic Faraday cage, and in the presence of desiccant (phosphorous pentoxide, P_2O_5; the presence of the desiccant, however, had no noticeable effect on the results).

The current density–applied field (j–E) dependencies for all types of films/cations were recorded for fields up to 20 kV m^{-1} (higher fields cause irreversible changes in the NP films and coalescence of the neighbouring nanoparticles[30]). In this range, the j–E dependencies were ohmic (Fig. 1e) and the conductivities of the films, $\sigma = j/E$, were constant for a given film type or condition (see Methods and Supplementary Section S2 for typical j–$V(t)$ curves at various concentrations of CH_3Hg^+). Before the immersion into the salt solutions, the conductivities of the striped EG_n particle films were $\sigma_{before} \sim 2 \times 10^{-4}\ \Omega^{-1}$ m^{-1}, which is close to the values previously recorded for films of Au NPs covered with thiolate SAMs of comparable thickness[30]. The conductivities increased (to σ_{after}) when the films were exposed to the cations (Fig. 1e). The degree of this increase depended crucially on the nature of the SAM coating the NPs, and on the nature and the concentration of the cations (Fig. 2). In all cases, the sensitivity of the sensors was defined as the concentration of cations in solution at which the ratio of the conductivities of the NP film, $\chi = \sigma_{after}/\sigma_{before}$, was greater than unity at the 99% confidence level (for statistical analysis, see Supplementary Section S3).

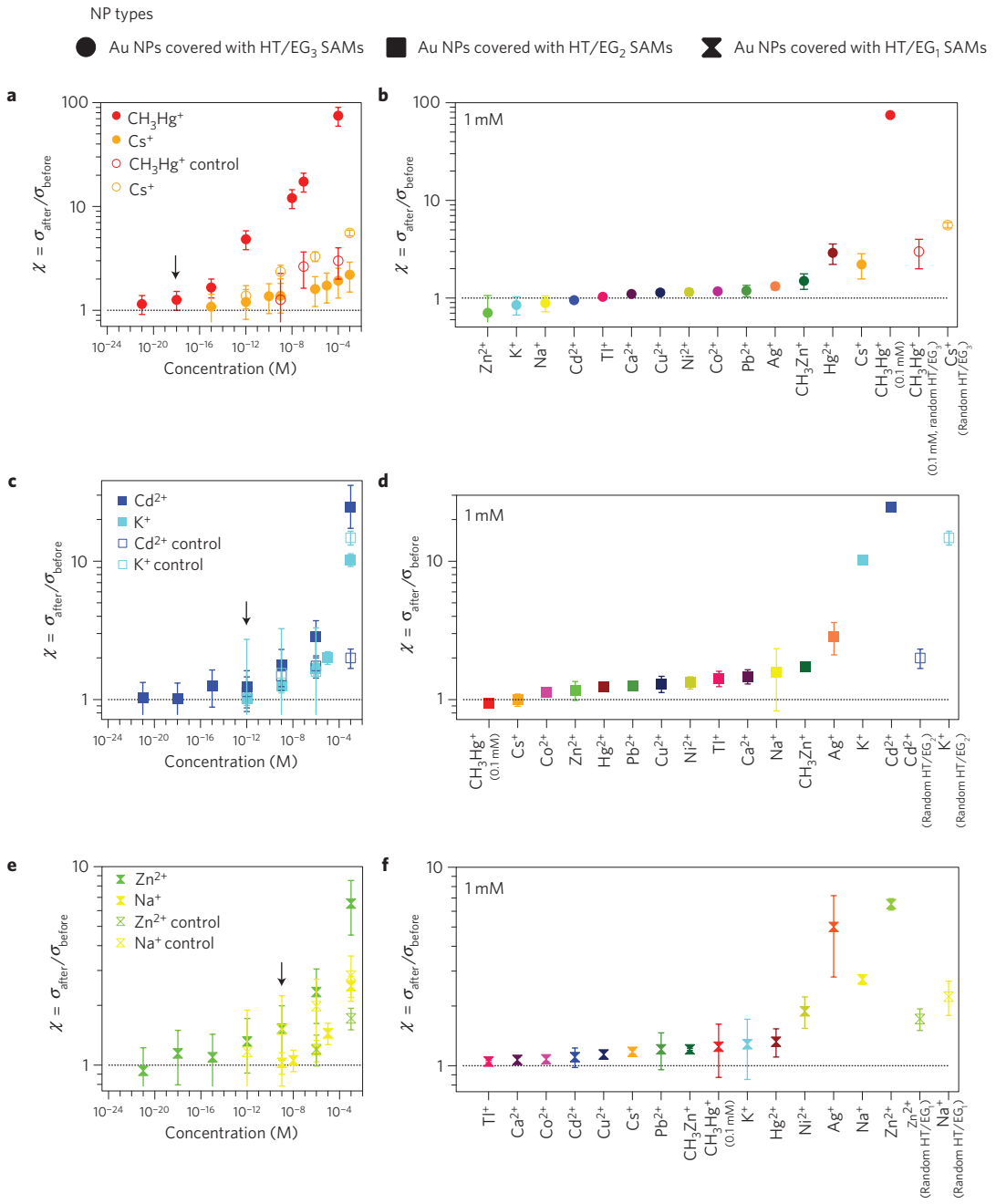

Figure 2 | Sensitivity (left column) and selectivity (right column) of cation sensing by different types of Au NPs decorated by HT/EG$_n$ SAMs. These measures are quantified by the change in the conductivities of the films on cation exposure, $\chi = \sigma_{after}/\sigma_{before}$. Filled symbols correspond to nanoparticles covered with striped HT/EG$_n$ SAMs; open symbols correspond to control experiments in which the nanoparticles were covered with disordered/non-striped SAMs of the same composition. Standard deviations are for at least 12 independent experiments for each condition. The arrows in the left column point to the detection limit/sensitivity (defined in the main text; see also Supplementary Section S3). **a**,**b**, Au NPs covered with HT/EG$_3$ SAMs detect CH_3Hg^+ selectively with a detection limit of ~1 aM. **c**,**d**, HT/EG$_2$ Au NPs detect Cd^{2+} and K^+ with a detection limit of ~1 pM for both cations. **e**,**f**, HT/EG$_1$ Au NPs detect Zn^{2+} and also Na^+ (detection limits: ~1 nM and ~1 μM, respectively). Note that the plots in **a**, **c** and **e** are double logarithmic and the conductivity increases nonlinearly with cation concentration.

Specifically, the HT/EG$_3$ striped Au NPs detected methyl mercury, CH_3Hg^+, with an approximately attomolar (10^{-18} M) sensitivity limit (corresponding to only ~600 CH_3Hg^+ cations in 1 ml of the surrounding solution; Fig. 2a). As the concentration of methyl mercury increased, χ increased nonlinearly with $[CH_3Hg^+]$ and reached a value of ~75 at $[CH_3Hg^+] = 0.1$ mM. Moreover, these sensing characteristics were selective for methyl mercury (Fig. 2b). For Co^{2+}, Pb^{2+}, Cu^{2+}, Ni^{2+}, Tl^+, Ca^{2+}, Ag^+, CH_3Zn^+, Cd^{2+}, K^+, Na^+, Cs^+ and Zn^{2+}, the conductivity did not change perceptibly ($\chi \approx 1$) over the entire range of concentrations tested; for Hg^{2+} and Cs^+ it changed only slightly ($\chi < 2.9$ and $\chi < 2.21$, respectively). Furthermore, for Cs^+, the detection limit was only ~1 μM—that is, 12 orders of magnitude above that of CH_3Hg^+.

Films of Au NPs coated with striped SAMs of HT/EG$_2$ detected Cd^{2+} with $\chi = 24.7$ at 1 mM and a detection limit ~1 pM (Fig. 2c,d). These NPs, however, also detected K^+ with $\chi = 10.2$ at 1 mM and with ~1 pM detection limit and, to a lesser degree, Ag^+

Table 1 | Film sensitivity and energies in cation complexation.

NP types	$\chi^{binding}$	$\chi^{non\text{-}binding}$	$\chi^{mixture}$
HT/EG$_3$	$\chi^{\mathbf{Cs^+}} = 1.600 \pm 0.512$	$\chi^{Na^+} = 0.888 \pm 0.165$	$\chi^{\mathbf{Cs^+}/Na^+} = 1.671 \pm 0.389$
HT/EG$_2$	$\chi^{\mathbf{Cd^{2+}}} = 2.859 \pm 0.858$	$\chi^{Zn^{2+}} = 1.170 \pm 0.182$	$\chi^{\mathbf{Cd^{2+}}/Zn^{2+}} = 2.373 \pm 1.238$
HT/EG$_1$	$\chi^{\mathbf{Zn^{2+}}} = 2.337 \pm 0.716$	$\chi^{Cd^{2+}} = 1.105 \pm 0.125$	$\chi^{\mathbf{Zn^{2+}}/Cd^{2+}} = 2.406 \pm 0.383$

Sensitivity (that is, $\chi = \sigma_{after}/\sigma_{before}$) in binary mixtures comprising cations that bind (denoted in bold) to the NPs and cations that do not bind (not bold). No significant differences between $\chi^{binding}$ and $\chi^{mixture}$ were observed. Standard deviations are for at least six independent experiments for each condition.

with $\chi = 2.86$. On the other hand, they did not bind Co^{2+}, Pb^{2+}, Cu^{2+}, Ni^{2+}, Tl^+, Ca^{2+}, CH_3Zn^+, Na^+, Zn^{2+}, Cs^+ and CH_3Hg^+. Finally, Au NPs coated with striped SAMs of HT/EG$_1$ were least selective and detected Zn^{2+}, Ag^+ and Na^+ (Fig. 2e,f). In this case, the values of χ were rather moderate (for example, at 1 mM, 6.51 for Zn^{2+}, 5.00 for Ag^+ and 2.72 for Na^+) although the sensitivity towards Zn^{2+} remained relatively high (for example, detection limit ~1 nM versus ~1 μM for Na^+). We note that Au NPs coated with random/non-striped HT/EG$_n$ SAMs were significantly less sensitive and in most cases less selective in detecting the highest-χ cations (but not some lower-χ cations, see open symbols in Fig. 2). Also, particles coated only with pure EG$_n$ SAMs exhibited even lower values of χ (for details, see Supplementary Section S4).

We emphasize that all χ values discussed above reflect the effects of cation binding and not any water and/or drying effects. This was verified in a series of experiments in which the films were washed in cation-free, deionized water and then dried—in this case, no statistically significant changes in the conductivities of the films were observed after either one or multiple wash/dry cycles (for example, for HT/EG$_2$ Au NP films, $\chi = \sigma_{after}/\sigma_{before} = 1.011 \pm 0.029$ after one cycle and 1.013 ± 0.031 after ten cycles). Also, when the cations were first captured into the films (such that conductivities increased) but were then washed off (by placing the films in 80 °C deionized water for 2–3 h), the conductivities returned to their native values before cation capture (see Supplementary Section S7). We observe that the films owe their robustness during all of these experiments (see Supplementary Section S6) to the crosslinking of the NPs by dithiols; films in which the NPs were not crosslinked simply dissolved when washed with or immersed in water.

The changes in the conductivity of the film result from the capture of the cations by the ligands on the NPs. This was directly verified by means of the ICP and X-ray photoelectron spectroscopy analyses of NPs before and after ion capture (see Supplementary Section S5 for these and other techniques used). In addition, Fourier transform infrared spectroscopy studies were performed that evidenced spectral changes on cation binding. Of particular importance here were the changes in the characteristic vibrational modes of the ethylene glycol units at 1001–1003 cm^{-1} and at 827 cm^{-1}. Remarkably, these changes were reversible in the sense that the original spectra were retrieved when the cations were washed off the NPs during immersion in 80 °C water (see above). These results also indicate that the capture of the cations is mediated by coordination-type interactions with the EG units, as should indeed be expected on the basis of common chemical knowledge. It is also worth noting that cations for which $\chi = \sigma_{after}/\sigma_{before}$ is close to unity do not cause significant changes in the NP/NP–film spectra as discussed in the Supplementary Section S5. Interestingly, a qualitatively similar result is obtained from solution experiments where the conductivities of NP suspensions are monitored during titration with different salt solutions. For those salts that are characterized by low χ in our solid-state (that is, NP–film) measurements, the conductance of NP solutions increases linearly with the amount of salt added; for those, however, that exhibit higher χ in NP films, the solution conductance initially remains constant, indicating that the added cations are trapped on the NPs (and thus do not contribute to the conductance of the solution; see Supplementary Section S5.5).

An essential feature of any chemical sensor is its selectivity, which in our case needs to be determined on exposure of NP films to cation mixtures. We first consider binary mixtures comprising cations that the NP films bind and sense with statistical significance (that is, giving conductance ratios $\chi = \sigma_{after}/\sigma_{before} > 1$ at 99% confidence levels) and cations that do not bind strongly and do not change conductivities at such confidence levels. Such pairs correspond to most of the possible combinations among the cations we tested (see Fig. 2). The results for some representative pairs are summarized in Table 1. Specifically, for the HT/EG$_3$ Au NP films, the presence of weakly binding Na^+ does not significantly change the signal coming from stronger binding Cs^+. Similarly, for HT/EG$_2$ Au NP films, the presence of Zn^{2+} does not strongly affect the signal due to Cd^{2+}, and for HT/EG$_1$ Au NP films the conductance on exposure to the mixture of Zn^{2+} and Cd^{2+} is close to the value characterizing the former cation. Such data confirm the selectivity of the films towards cations giving larger values of χ. Moreover, the signals from the NP–film sensors are not affected by the changes in the ionic strength of the solution due to the non-binding, low-χ cations (see Supplementary Fig. S9a).

Of course, the selectivity decreases when the films are exposed to mixtures of cations characterized by similar $\chi > 1$ values (Supplementary Section S12). This problem is the least pronounced for HT/EG$_3$ Au NP films (see Fig. 2 and Supplementary Section S8), which are therefore suitable for deployment as environmental CH_3Hg^+ sensors. This is illustrated in Fig. 3, where we used our sensors to measure the CH_3Hg^+ content in environmental samples directly relevant to the issues of public health—tap water, lake water and fish (see Methods for detailed preparation and analysis of environmental samples). Importantly, the results we obtained for the lake water could be directly compared to the values reported in the literature for the same lake (Lake Michigan) sample, and the CH_3Hg^+ content in fish could be compared to the value determined by the United States Geological Survey (USGS). For the lake water, our measurements gave a 5.9 fM concentration of CH_3Hg^+ (range within one s.d. 0.35–43.3 fM) versus 5–210 fM reported in ref. 38. For the fish, we measured a concentration of 3.81 pM (range within one s.d.: 1.62–8.19 pM), in excellent agreement with the 3.58 pM value provided to us by the USGS after our experiments were completed. A reassuring result—at least for the citizens of Evanston—is that the content of CH_3Hg^+ in the tap water of this city is very low (27.7 aM, range within one s.d.: 4.5–138 aM). We make two further comments about all of these results. First, when the environmental samples were spiked with known concentrations of CH_3Hg^+, the readings of our films fell onto the calibration curve obtained using the concentration standards (that is, solutions of CH_3Hg^+ in pure, deionized water)—this means that there is no background interference from components other than CH_3Hg^+ in the environmental samples. Second, we emphasize that our

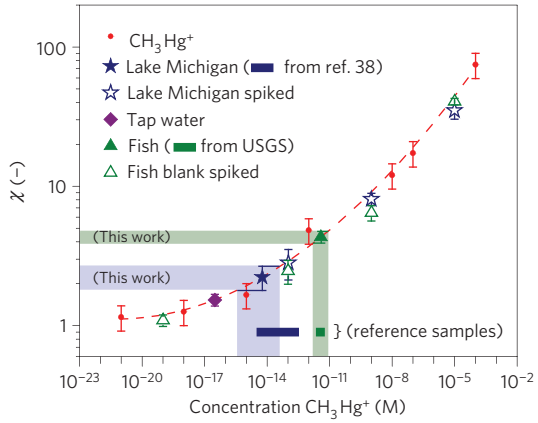

Figure 3 | Selectivity of the films on exposure to cation mixtures and environmental samples. The χ values measured for the environmental samples (blue star: water from Lake Michigan, purple diamond: Evanston tap water, green triangle: mosquito fish collected by USGS from Everglades National Park). Red symbols correspond to the measurements of standard solutions (that is, of known CH_3Hg^+ concentration in deionized water) and the dashed calibration curve is the second order polynomial fit. Open symbols correspond to the environmental samples 'spiked' with known amounts of CH_3Hg^+. Pale green and pale blue regions correspond to the one-standard-deviation ranges in our measurements (three different films, at least six measurements per film) of, respectively, fish and lake water samples. Dark green horizontal bar corresponds to the range of CH_3Hg^+ content in the mosquito fish determined by USGS, and the dark blue horizontal bar corresponds to the one-standard-deviation range of CH_3Hg^+ concentration in Lake Michigan determined in ref. 38. For further experimental detail, see Methods.

Table 2 | Film sensitivity and energies in cation complexation.

NP/cation types		HT/EG_1	HT/EG_2	HT/EG_3
Free		9.160	9.143	9.142
Zn^{2+}	Intra	1.834	2.408	3.098
	Inter	**1.398**	1.976	3.031
Cd^{2+}	Intra	4.395	3.969	4.088
	Inter	3.928	**3.676**	4.243
CH_3Hg^+	Intra	**6.045**	6.392	6.272
	Inter	6.154	6.129	**6.045**

Calculated energies of the HOMO/LUMO gaps (in eV) for different cations and EG_n thiols. 'Interband' corresponds to the situation where the cations are bound at the edge of an EG_n stripe; 'intraband' corresponds to the cation being placed within one EG_n band. Entries in bold correspond to minimal gap energies for a given type of EG_n and generally agree with/reflect the cation-binding selectivity observed in experiments.

results were achieved in a technically straightforward manner (by simply dipping the film in the sample solution), in contrast to other methods that require tedious sample pretreatment, including conversion of methylmercury to ethylmethylmercury and concentration on a dedicated column before analysis by gas chromatography combined with ICP mass spectrometry[2,39].

We now turn our attention to the fundamental aspects of the relationship between the binding of cations into the film and the observed current changes. There are two interrelated components that need to be considered: cation-facilitated electron transport through the molecular bridge between proximal NPs, and formation of the conductive paths through the film, which ultimately give rise to the high sensitivity of the cation detection. To understand the electronic structure of the bridge, we performed quantum-mechanical calculations for a fragment of NP surface comprising two nearby EG_n stripes and an HT stripe between them (Fig. 4a). Calculations were performed for both the cation-free HT/EG_n systems, as well as a system in which different metal cations were placed either within the EG_n stripes (denoted intra in Table 2) or at the edges of these stripes (inter). In all cases, the geometry of the system was optimized by a semi-empirical quantum-mechanical method NDDO-PM6 (ref. 40; with the MOPAC2007 (ref. 41) software) at the Non-equilibrium Energy Research Center supercomputer centre. The calculations indicate that the experimentally observed selectivities do not correlate with the calculated energies of the complexation of the cations by various HT/EG_n Au NPs or with the heats of formation of these complexes, nor with the energies of the highest occupied molecular orbital (HOMO) or the lowest unoccupied molecular orbital (LUMO). On the other hand, the observed cation selectivities can be related to the HOMO/LUMO gap, ΔE (Table 2). This result suggests that both HOMO and LUMO orbitals are involved in electron transport. Although this is not a typical scenario in describing conduction through a molecular bridge[42], similar models have been used previously to describe transport through disordered media (as our films are)[43]. In this context, we observe that in our system the HOMO orbital (and other high-energy occupied orbitals) is always located close to the NP surface (Fig. 4b), whereas the LUMO orbital (and unoccupied orbitals close to it) is mostly centred on the EG_n/cation fragments (Fig. 4c). Therefore, for the electrons to travel through the SAM, they must be injected from the HOMO into the LUMO. Importantly, the energy required for this injection is substantially diminished on cation binding, and the smallest values of ΔE generally reflect the detection specificity observed in experiments: for Zn^{2+}, the smallest ΔE corresponds to the binding to the HT/EG_1 Au NPs; Cd^{2+} has the smallest ΔE when binding to HT/EG_2 Au NPs; for CH_3 Hg^+, ΔE is the least when binding inter-stripe to HT/EG_3 Au NPs (although, in this case, calculations give the same value for HT/EG_1 particles; Table 2). We note that for any given HT/EG_n/cation system, the ΔE gaps (and the absolute binding energies) are typically lower when cations coordinate with ethylene glycols at the edges of the EG_n stripes than when these cations are fully buried within the EG_n stripes. This observation suggests that the free space provided by the HT stripes is important for the operation of our sensors (as also corroborated by molecular dynamics simulations illustrated in Fig. 4d and Supplementary Section S9).

The decrease in ΔE on cation binding increases the electronic conductance of a NP-SAM//SAM-NP molecular bridge, $\sigma_c \propto (e^2/h)(e^{-2(m\Delta E)^{1/2}L/h})^2$, where h is Planck's constant, m is the rest mass of an electron and L is the thickness of the NP ligand shell[44]. Importantly, as multiple cations bind into the NP film, the local changes over individual bridges can translate into a global change in the conductance of the film. This process can be described by combining σ_c with the cation-binding kinetics and Bruggeman's effective medium theory[45,46] (EMT) accounting for the formation of conductive paths percolating the NP film (Fig. 5a,b). The binding of cations to the EG_n ligands as a function of concentration $[C]_0$ can be described in terms of the Sips isotherm[47]: $\theta = (K_{eq}[C]_0)^a/[1 + (K_{eq}[C]_0)^a]$, where θ is the fraction of occupied sites, K_{eq} is the equilibrium association constant and a is the heterogeneity index. The Sips isotherm is a composite of the familiar Langmuir isotherm ($\theta_{LM} = K_{LM}[C]_0/[1 + K_{LM}[C]_0]$) and the Freundlich isotherm ($\theta_F = K_F[C]_0^{1/n}$), commonly used for low-concentration binding in heterogeneous systems. The Sips isotherm approaches Langmuir's formula for a close to unity and Freundlich's equation at low concentration, and has been used to describe ligand binding to powders[48] and aggregated nanoparticle media[49]. The heterogeneity index (a) determines the width of the Gaussian-like distribution of K_{eq}, which arises from steric effects, conformational changes and differences in the chemical microenvironment[50]. Using the